Chapter 2

Retinal Vasculature Identification and Characterization Using OCT Imaging

Joaquim de Moura, Jorge Novo, José Rouco,
Noelia Barreira, Manuel Penedo and Marcos Ortega

Additional information is available at the end of the chapter

http://dx.doi.org/10.5772/intechopen.78292

Abstract

The eye fundus is the part of the human body where the blood vessels can be directly observed and studied. For this reason, the analysis and diagnosis of many relevant diseases that affect the circulatory system, for example, reference, hypertension, diabetes or arteriosclerosis can be supported by the use of this source of information, analyzing their degree of severity and impact by the study of the properties of the retinal microcirculation. The development of computer aided-diagnosis tools became relevant over the recent years as they support and facilitate the work of specialists, helping to accurately identify the target structures in many processes of analysis and diagnosis. In that sense, the automatic identification of the retinal vasculature is crucial as its manual identification is an exhaustive and tedious work when it is manually performed by the experts. This chapter presents an analysis of the characteristics of the optical coherence tomography imaging and its potential for the retinal vascular identification and characterization. In that sense, we also analyze computational approaches to automatically obtain and characterize the retinal vasculature and provide an intuitive visualization that facilitates the posterior clinical analysis of relevant diseases such as hypertension or diabetes.

Keywords: computer-aided diagnosis, retinal image analysis, optical coherence tomography, vasculature, retinal microcirculation

1. Introduction

The analysis of the eye fundus is widely used by clinical specialists to identify, analyze and characterize different morphological relevant structures such as the optic disc, the macula

or the arterio-venular vasculature. These clinical evaluations allow the doctors to detect and treat different systemic diseases that affect the circulatory system, for example, hypertension [1], diabetes [2] or arteriosclerosis [3]. Considering the high prevalence and the possible consequences that are directly associated with these diseases, the analysis and monitoring of the retinal microcirculation represents an important task in the diagnostic process [4]. A precise evaluation of the retinal vasculature permits the early identification of several clinical conditions that facilitate an appropriate diagnosis and treatment as well as their prevention [5].

The retinal vessels not only proved their potential in clinical procedures but also in other purposes. Thus, the structure of the retinal vasculature also demonstrated its potential viability as an alternative model for a biometric authentication system [6]. This is due to the complex structure of the retinal vessels, which is unique for each person. Hence, the patterns that were typically used in the identification process are the landmarks of the vasculature [7]. Typically, bifurcations and crossovers are obtained from the retinal vessel tree and used in the identification process [8].

Nowadays, computer-aided diagnosis (CAD) systems are frequently used to improve the accuracy and consistency of different clinical evaluations, facilitating the work of the experts in many relevant diagnostic processes and replacing manual procedures that are tedious and highly time-consuming [9]. These independent decision systems are significantly helpful in the interpretation of several types of medical images, which simplify the doctor's everyday work and improve the quality of patient diagnosis and treatment [10].

Among the different retinal image modalities, optical coherence tomography (OCT) imaging is increasingly in use in clinical services [11]. This imaging modality increased its popularity over the recent years by offering cross-sectional visualizations of the retinal tissues and other relevant structures with a high-resolution and in a reliable noninvasive manner [12]. This technique provides real-time images that are frequently used in the detection, analysis and evaluation of different retinal diseases as, for example, age-related macular degeneration or diabetic retinopathy, which are among the major causes of blindness in the developed countries [13].

The OCT capture technique is based on the principle of the Michelson interferometer to produce the cross-sectional OCT sections, by sequentially collecting reflections from the lateral and longitudinal scans over the retina [14]. The set of OCT sections is complemented with the corresponding near-infrared reflectance (NIR) retinography. Both images are typically captured simultaneously with the OCT capture device by being directly provided to the user for their posterior inspection and use. **Figure 1** shows a representative example of OCT image composed by the NIR image and a corresponding OCT section.

The OCT imaging technique is widely used in the area of ophthalmology, given the facility with which light penetrates in the main ocular structures in both the anterior and posterior segments of the eye [15]. The complete set of information that is provided by this image modality allows the experts to perform a more reliable analysis of the retinal microcirculation that is needed in many processes of diagnosis, treatment and corresponding clinical monitoring [16]. For that reason, a two-dimensional and three-dimensional analysis of the retinal vessel tree in OCT images offers a more precise and coherent information about possible abnormal changes in the retinal vascular architecture that may be derived by a large variability of pathological conditions.

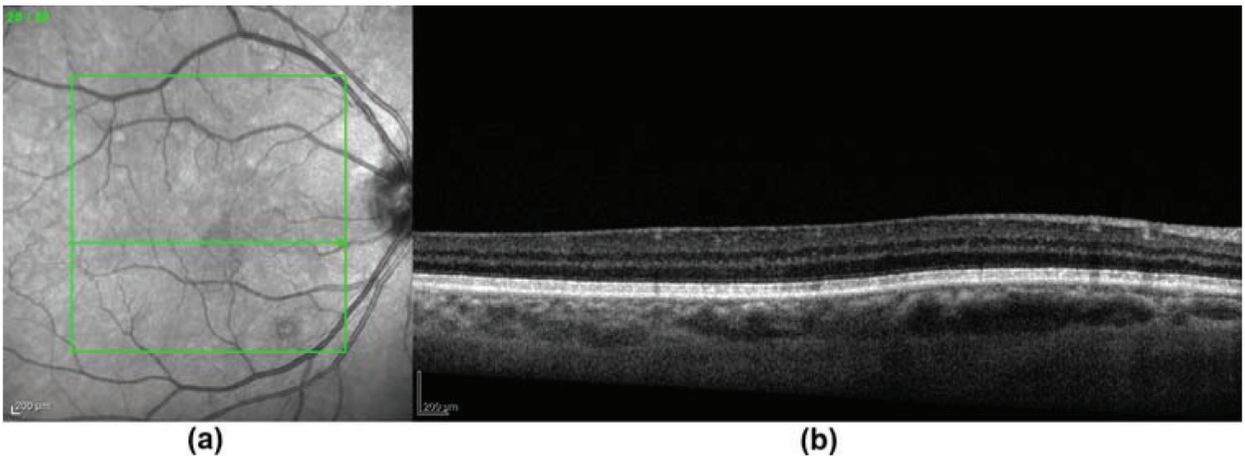

Figure 1. Example of OCT scan. (a) Near-infrared reflectance retinography image and (b) OCT histological section.

In this chapter, we provide an analysis of the characteristics of the OCT image modality and its potential for the retinal vessel tree identification and characterization, which are necessary for many clinical assessments, diagnoses and treatments. In addition, we present a representative computational approach for the automatic detection and characterization of the retinal blood vessels in OCT images, which is combined with an intuitive visualization tool that facilitates the posterior analysis by the clinical specialist in a large variability of diseases. Thus, we motivate the implementation of computational systems and the suitability of the analysis and visualization of their output results.

Section 2 describes the approaches including the extraction of the retinal vasculature and their posterior two-dimensional or three-dimensional reconstruction and visualization. Finally, the conclusion drawn in Section 3 closes this chapter.

2. Automatic extraction and visual reconstruction of the retinal vasculature

The representative system herein described for the vascular extraction and visualization is organized in a set of progressive stages. Firstly, the presence of the retinal vessel tree is automatically identified using the OCT images. In particular, the NIR image and/or the OCT histological sections are analyzed to identify the presence of the vascular structures. Subsequently, the calibers and depth of the vascular profiles are measured. Finally, we use the entire set of extracted information to make a graphical two-/three-dimensional representation, providing an intuitive visualization tool of this complex vascular structure. **Figure 2** illustrates the main parts of the methodology, each stage being detailed in the following subsections.

2.1. Characteristics and variability of the input optical coherence tomography images

Typically, the system receives, as input, a set of OCT images. These images correspond to high-resolution images of the different retinal layers over the macula region approximated

by the histological sections. As said, the OCT scan is composed of the NIR image as well as the consecutive OCT histological sections that are often simultaneously obtained by the same capture device, providing sets of images, as illustrated in **Figure 1**. Using these images, we delimited the region where the retinal vessels are located in both modalities.

Recently, several companies have invested in research in the field of ophthalmology especially in the development of OCT capture devices with significant software improvements [17]. Four of the commonly used OCT devices in the daily medical practice are the Cirrus (Carl Zeiss Meditec, Dublin, CA, USA), the Spectralis (Heidelberg Engineering, Heidelberg, Germany), the RTVue (Optovue, Fremont, CA, USA) and the Triton (Topcon, Tokyo, Japan) models. The working principles are similar for all these OCT capture devices; however, they can differ slightly in precision, throughput, depth penetration, acquisition speed, data processing and resolution [18].

In this chapter, we present approaches that were validated mainly with OCT images that are provided by the Spectralis model. Using this OCT capture device, the scan acquisition

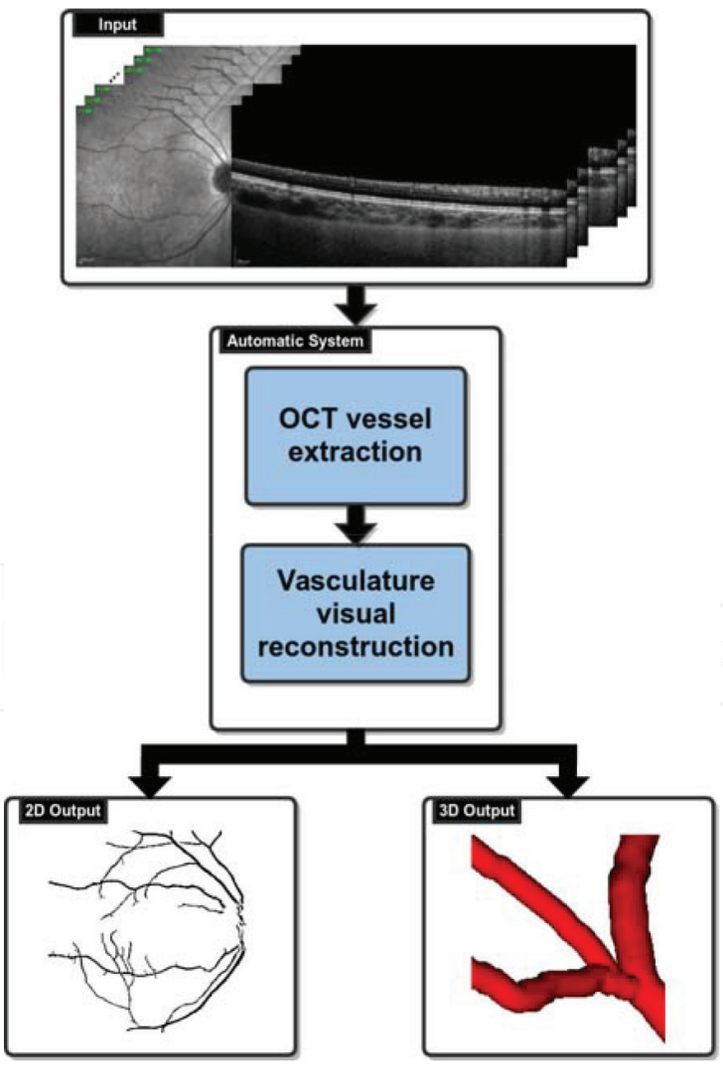

Figure 2. Scheme of the vascular extraction and reconstruction system.

was done by selecting the dense volume scan type over a scan angle of 20°×20°, roughly 6 mm × 6 mm, consisting of 49 B-mode scans acquired utilizing Automatic Real-Time (ART Mean) = 16 (number of scans averaged). B-mode scans are separated by 120 μm from each other and are composed of 1024 A-mode scans, with a separation of 5.5 μm. Each A-mode scan has 496 pixels with 3.8 μm resolution. The system acquires the images at a given frame-rate (8.8 frames/s) and with a given bit depth (32-bits). The approaches herein presented were validated using image datasets including OCT scans with these characteristics. As we can see in the results of the corresponding articles [19, 23], both were satisfactorily tested, demonstrating their suitability for the analyzed issue.

2.2. OCT vessel extraction

Most of the times, the computational systems are provided with both NIR/histological sections. However, there are scenarios where the systems have to perform the analysis with only the availability of the OCT histological sections. For that reason, in this stage, we describe two different and independent approaches for the automatic identification and extraction of the retinal vascular structure, depending on the factor regarding the amount of information of the OCT images provided (see **Figure 3**). The first approach uses the information provided by the NIR image in combination with the histological sections, while the second approach uses only the OCT histological sections for the identification and characterization of the vessel profiles. The characteristics of each approach is detailed in the following subsections.

2.2.1. Vessel extraction using the combination of the near-infrared reflectance image and the histological sections

First, we present a proposal for the identification and segmentation of the retinal vascular structure using the NIR image combined with the histological section images. Generally, the system performs a 2D identification of the vasculature using the NIR image, where we extract the retinal vessel tree and, after that, we obtain the vessel centerline representation. Next, the corresponding calibers of each centerline coordinate are measured. Finally, these identifications are mapped in the corresponding positions of the histological sections to calculate the vascular depths of each vessel coordinate (see **Figure 4**).

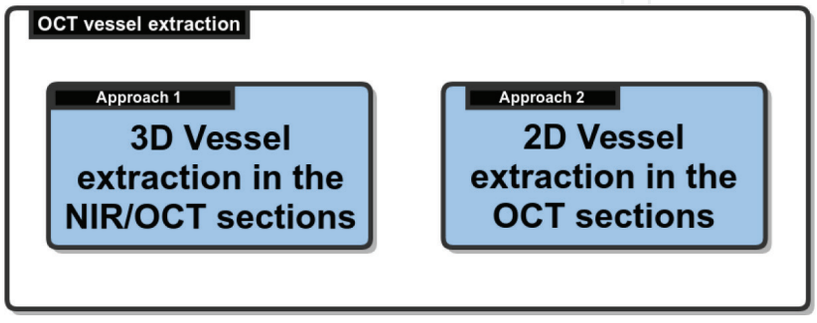

Figure 3. Vessel extraction in OCT images by two different approaches using NIR/OCT sections or only OCT sections.

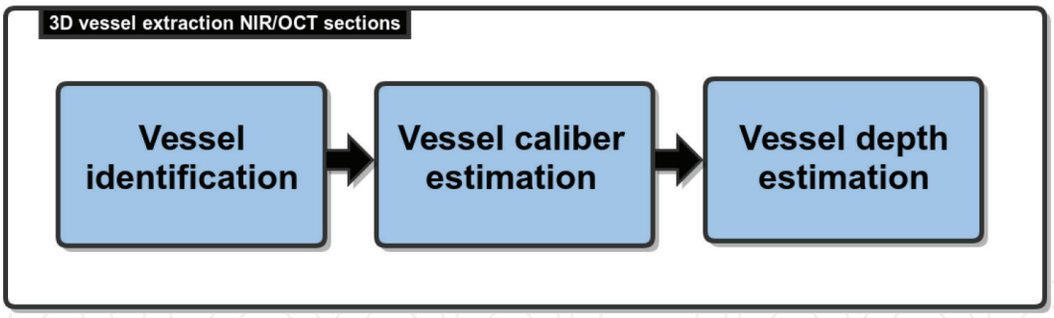

Figure 4. Scheme of 3D vessel extraction using the combination of NIR and the histological sections.

2.2.1.1. Vessel identification

Initially, a preprocessing stage is performed to enhance the biggest and darkest structures that characterize the vessels in the NIR images [19]. To achieve this, we use a morphological top-hat transformation (see **Figure 5(b)**). Then, the noise and the vascular reflex are reduced with a median filter (see **Figure 5(c)**). This process facilitates the posterior extraction of the retinal vessels and reinforces the robustness of the method [20].

An initial segmentation was performed by means of a hysteresis-based thresholding technique [21]. A hard threshold (T_h) represents pixels with a high probability of being blood vessel pixels while a weak threshold (T_w) keeps all the pixels of the vascular tree in the surrounding region, even spurious ones. The final segmentation is formed by all the pixels that were included by the T_w threshold connected to, at least, one pixel obtained by the T_h threshold. The values for T_h and T_w are extracted from two characteristics calculated on the NIR images: the percentage of vascular tree and the percentage of background. These thresholds are calculated using percentile values, according to (Eq. (1)).

$$P_k = L_k + \frac{k(n/100) - F_k}{f_k} \times c, \quad k = 1, 2, \ldots, 99 \tag{1}$$

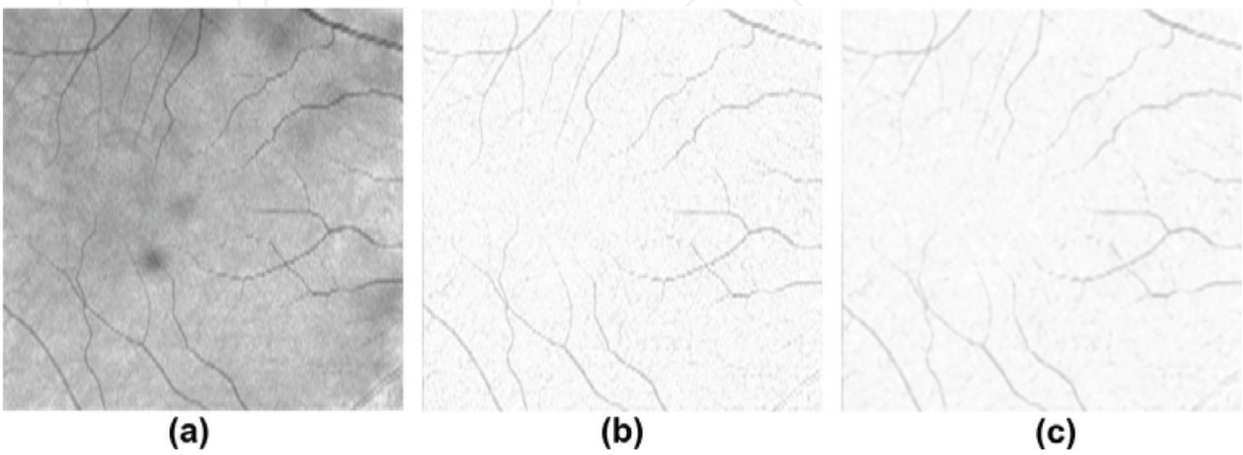

Figure 5. Example of the preprocessing stage in the NIR. (a) Input NIR retinography image; (b) morphological top-hat transformation result and (c) median filter result.

where L_k is the percentile lower limit k, n is the size of the data set, F_k is the accumulated frequency for k - *1* values, f_k depicts the frequency of percentile k and c is the measurement of the size of the percentile interval. In our case, c is equal to 1. A representative example of the vessel segmentation stage using an NIR retinography image is presented in **Figure 6(b)**.

Next, we proceed to identify the centerline of each vessel segment using as baseline the information that was obtained in the previous segmentation. The retinal vessel centerline identification is done using a crease-based strategy. This method follows the idea that vessels can be thought of as creases (ridges or valleys) when images are seen as landscapes [22]. This way, the Multi Local Set of Extrinsic Curvature enhanced by the Structure Tensor (MLSEC-ST) operator is applied with this aim. Then, a skeletonization method is applied to obtain the vessel centerline representation of each vessel by means of one-pixel width segments, as we can see in **Figure 6(c)**.

2.2.1.2. Vessel caliber estimation

In addition to the vessel centerline coordinates, we also need to determine their calibers at each point of the vessel segments, in order to obtain a coherent three-dimensional representation of the retinal vessel tree (see **Figure 7(a)**). The vascular caliber is calculated for each vessel coordinate as the distance between their edges (see **Figure 7(b)**). To this aim, we use the information of the achieved segmentations and the vessel centerlines. These values were previously estimated in the segmentation stage. The vessel orientation θ is calculated as the angle between two consecutive vessel points: $P_1(x_1, y_1)$ and $P_2(x_2, y_2)$. The caliber is then estimated in the perpendicular direction of this angle, see (Eq.(2)).

$$\theta = \arctan\left(\frac{y_2 - y_1}{x_2 - x_1}\right) \tag{2}$$

2.2.1.3. Vessel depth estimation

The depth estimation of the retinal vessels is calculated using the depth information that is provided by OCT histological sections. The shadow projections on the retinal layers indicate

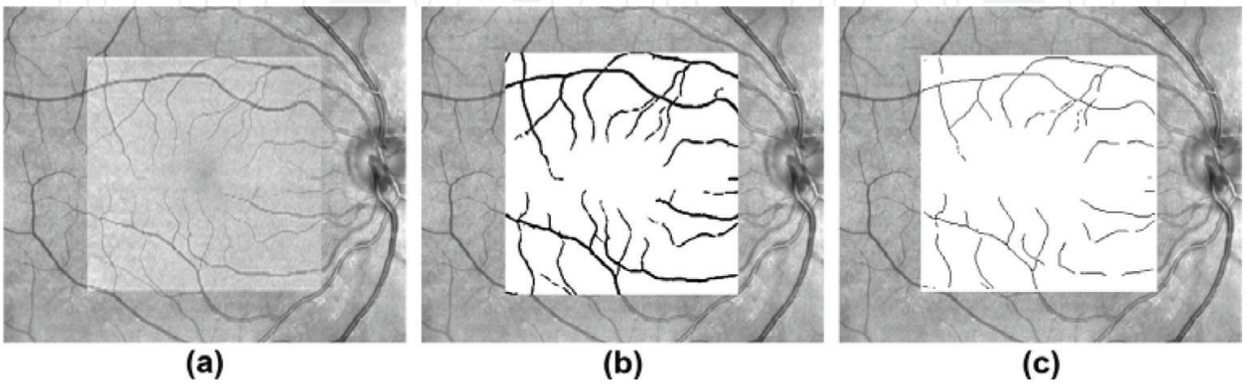

Figure 6. Example of the vessel extraction stage in NIR image. (a) Input NIR retinography image; (b) vessel tree segmentation and (c) vessel tree centerline identification.

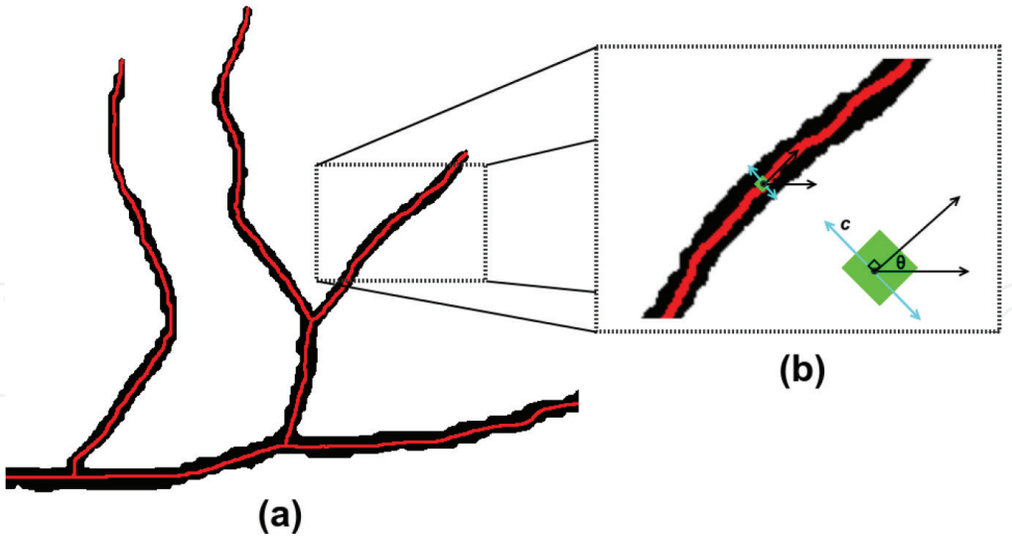

Figure 7. Example of the vessel caliber estimation stage. (a) Vessel centerline overlapping the vessel segments and (b) representation of the analyzed direction at each point of a vessel segment.

the presence of the vessel profiles. In the OCT histological sections, the vessel profiles are the bright spots situated between the retinal layers. To detect these spots, we make a previous mapping process to delimit the vascular region in the OCT section, as is illustrated in **Figure 8**. Then, a search process is performed in this region to determine the precise location of these vessel profiles. The vascular depth Z is estimated by the distance between the vessel profile C_v and the retinal pigment epithelium (RPE) layer P_i, see (Eq.(3)).

$$Z = |C_v - P_i| \tag{3}$$

2.2.2. Vessel extraction using only the OCT histological sections

In many occasions, computational tools are not provided with the entire set of NIR retinography images in combination with their corresponding OCT histological sections. Given this

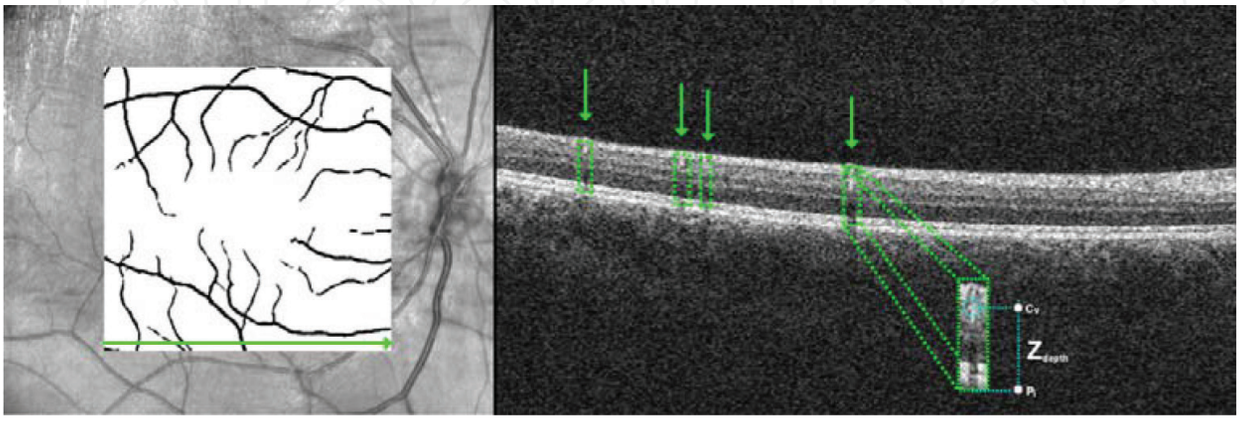

Figure 8. Example of the vessel depth estimation stage with the mapping process and the delimitation of the vascular region.

frequent scenario, that constitutes a limitation, another proposal is also detailed for the automatic detection of retinal vessels using, only, the information that is obtained through the OCT histological sections [23]. To achieve this, the tool bases its performance on the exploitation of the information provided by the shadow projections of the vessels along the retinal layers to identify the presence of vascular structures (see **Figure 9**).

The eye fundus presents a layered structure that contains five main cell types: photoreceptor, horizontal, bipolar, amacrine and ganglion [24]. These cells present different responses to the reflection, transmission and absorption of the light stimuli that are emitted by the OCT capture device. Given this, the presence of the vascular shadows is more prominent in some retinal layers given their brightness, facilitating the detection of the vessel profiles in the OCT sections. In particular, this information is more visible in the region between the Pigment Epithelium Bruch's Complex and the Choroid (RPE/C) layer and the top boundaries of the Ellipsoid (M/E) layer. To achieve the identification of these retinal layers, the method implemented an automated approach using snakes, an active contour-based model [25]. Snake strategies are one of the most common methods that are used in segmentation problems in many issues of medical imaging. This active contour-based model bases its performance on the fact that each vertex of the snake is moved according to inner and outer forces, and the general contour turns stable when the model reaches its local minimum. The mathematical snake model is shown in (Eq.(4)).

$$\xi_{snake}(s) = \int \xi_{internal}(s)ds + \int \xi_{external}(s)ds \tag{4}$$

The interaction between the snake energies are measured by the energy function ξ_{snake} where $\xi_{internal}$ represents the elasticity energy and $\xi_{external}$ measures the energy of the snake when finding the intensity edges. In **Figure 10**, we can see a representative example with the identification of the RPE/C and M/E retinal layers, delimiting the region of interest where the vascular shadows are identified easily.

Using this identified region of interest, a preprocessing stage is carried out to increase the robustness of the vascular shadow identification process to possible changes in contrast and brightness, a situation that is frequent in OCT images (see **Figure 11**). First, a Gaussian blurring filter is employed to remove the characteristic speckle noise of these images. Next, a

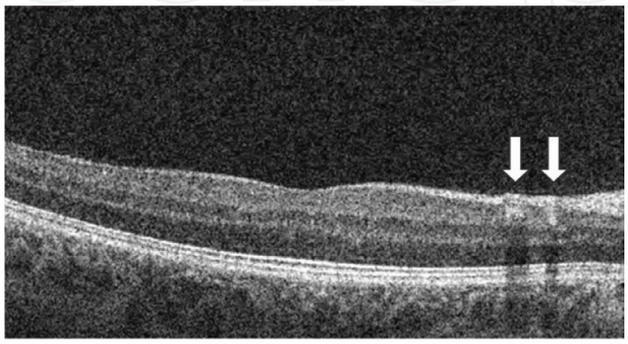

Figure 9. OCT section with the shadow projections of a couple of vessels.

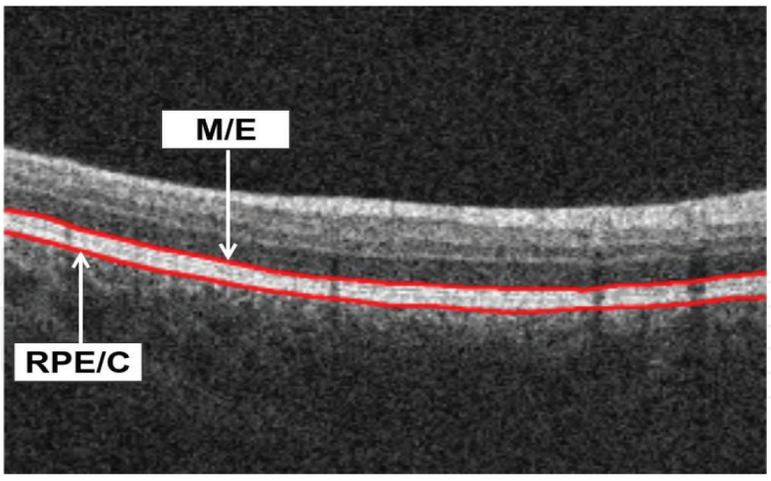

Figure 10. Example of OCT histological section with the identification of the two aimed retinal layers: RPE/C and M/E.

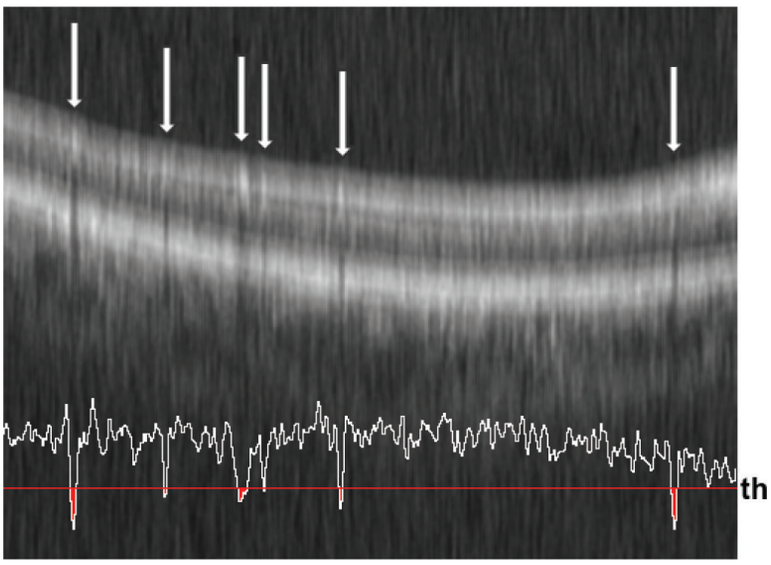

Figure 11. Example of preprocessed OCT section where the vessel profiles are graphically represented as valleys in the mean intensity signal and detected in the region below a fixed threshold.

morphological top-hat transformation is used to enhance the contrast of the vascular shadows. Finally, we calculate the statistical features in the region of interest, features that are used to identify the vascular presence. To achieve this, we analyze the intensity profiles of the vessel shadows in this region. These intensity profiles are calculated using a derived signal, where each point represent the mean of the intensity in each column that is delimited by the mentioned layers RPE/C and M/E. The vessel profiles are identified by means of existing significant local minima along this signal. To achieve this, we use as selection criteria a model that employs a fixed threshold, *th*, as shown in (Eq.(5)).

$$th = \frac{3}{2}(Q_3 - Q_1) + Q_3 \tag{5}$$

where Q_1 represents the first quartile and Q_3 represents the third quartile. As shown in **Figure 11**, the vessel profiles are graphically represented as valleys and detected in the region below a fixed threshold.

2.3. Vasculature visual reconstruction

Nowadays, automatic visualization systems are commonly used by clinical specialists to perform the diagnosis, monitoring and treatment of many diseases. In particular, OCT images provide detailed and relevant information that can be used in the analysis and posterior reconstruction of the retinal vessel tree. Depending on the input image of our system (NIR and/or histological sections), we can obtain more or less information about the characteristics retinal vasculature. Based on the information that is provided by the input scan, we perform the corresponding two-dimensional or three-dimensional visual reconstruction, as we explain in the following sections.

2.3.1. 2D vascular reconstruction

In this stage, we use the information of the vessel profiles that was obtained from a set of OCT histological sections. The information provided by these vascular profiles is used to perform the two-dimensional reconstruction of the entire retinal vessel tree.

First, we make a preliminary binary vessel map with all the vessel profiles that were identified using a set of OCT scans. In this vessel map, each row represents the vascular information obtained for each OCT scan. Then, we scale this binary vessel map to obtain a final representation of the vascular structures with the same dimensions of the original scan (see **Figure 12(a)**). The scaling process is done using the separation value between each OCT scan, if available. This value is a parameter that is selected in the OCT capture device by the clinical expert in the process of obtaining the OCT scans. And finally, we make a two-dimensional reconstruction of the retinal vessel tree using the final binary vessel map obtained, as we can see in **Figure 12(b)**. In this example, we can observe the final two-dimensional identifications over the existing NIR image, for a better illustration of the performance of the approach, despite it not being employed in the identification process.

2.3.2. 3D vascular reconstruction

In this section, we use the information of the vessel profiles provided by the NIR and the histological sections to produce a visual vascular three-dimensional representation. The system represents each vascular structure as a segment S, where each point P of the vascular segment S is represented by the coordinates (x, y, z) and the vessel calibers d, values that were previously calculated [26]. Then, an interpolation by B-splines $S(u)$ is used with the entire set of points P_i connecting them in a curve, see (Eq.(6)).

$$S(u) = \sum_{i=0}^{n} B_{i,m}(u) P_i \quad 2 \leqslant m \leqslant n+1 \tag{6}$$

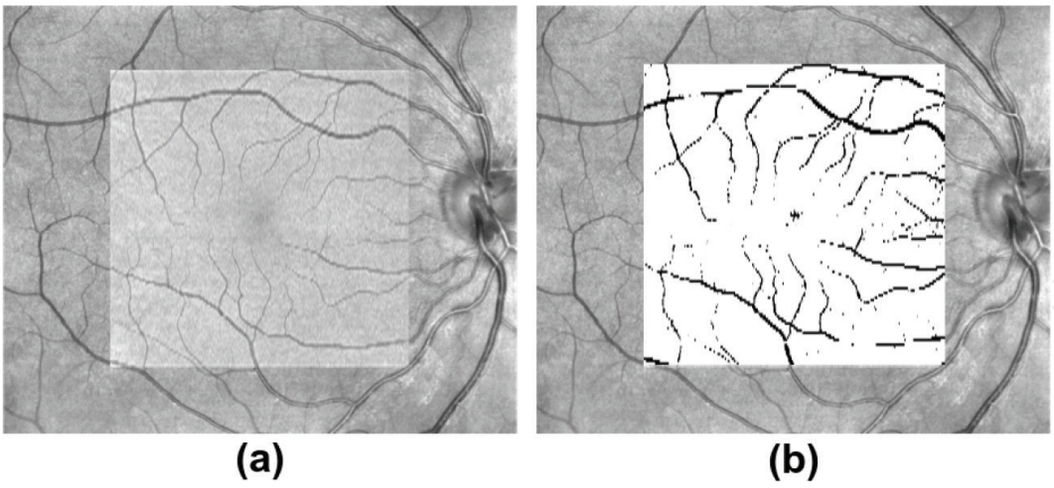

Figure 12. Example of the vessel extraction results in using the approach that uses only the OCT histological sections. (a) NIR retinography image and (b) two-dimensional vascular reconstruction using the vascular identifications.

where P_i is the ith control point of the $(n + 1)$th control point of the curve and $B_{i,m}$ are the B-spline functions, which are polynomials of degree $m - 1$. **Figure 13** shows a representative example of the interpolation process with B-spline curves.

Each vascular segment is represented with a tubular shape centered in the corresponding coordinates (x, y, z) and with a diameter equivalent to its caliber, d. Subsequently, a postprocessing is performed to smooth the transitions between the consecutive vascular coordinates and, therefore, allow a more reliable representation of the vascular structure [27]. **Figure 14** shows this three-dimensional representation process over a given curve.

Finally, this automatic system allows a complete three-dimensional visualization of the complex retinal vessel tree by means of graphical affine transformations including translation,

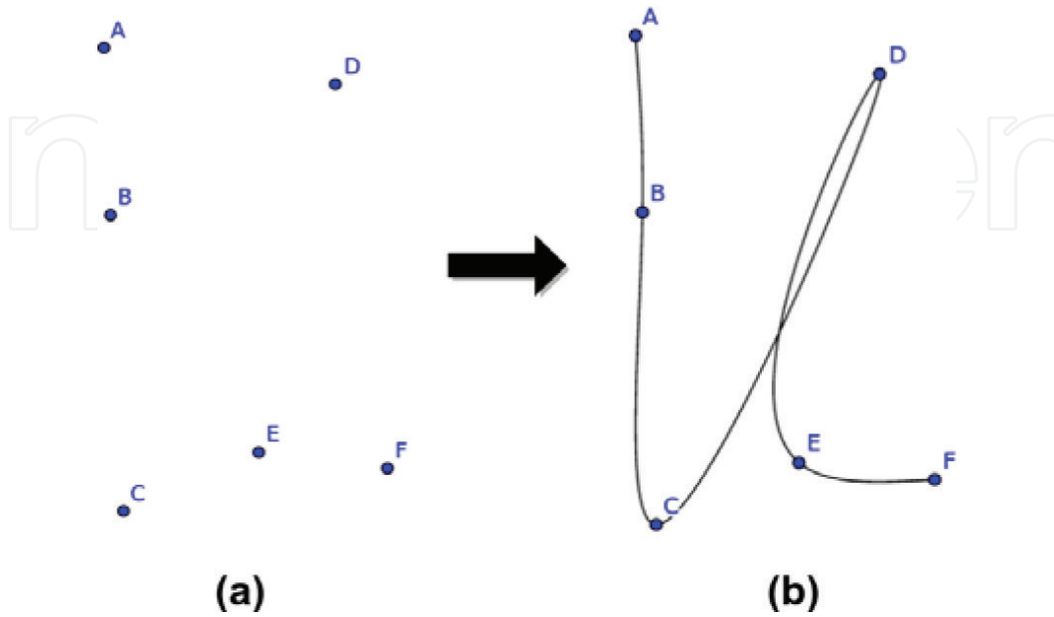

Figure 13. Example of the interpolation process. (a) Set of Cartesian coordinates (x, y, z) and (b) interpolation with B-spline curves between the set of Cartesian coordinates.

http://dx.doi.org/10.5772/intechopen.78292

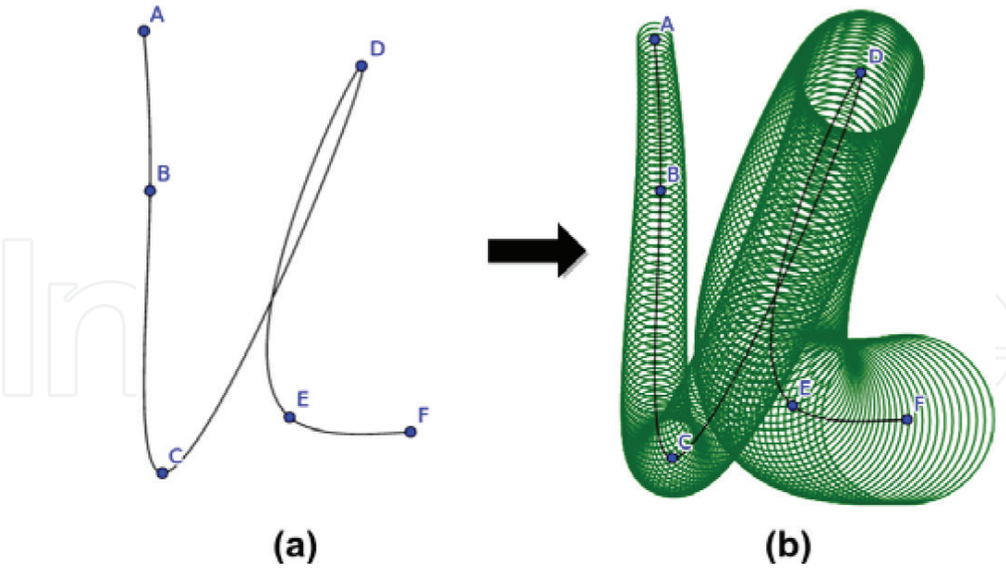

Figure 14. Example of the three-dimensional representation process. (a) Interpolation with B-spline curves between Cartesian coordinates. (b) Representation of a 3D tubular structure associated with the curve.

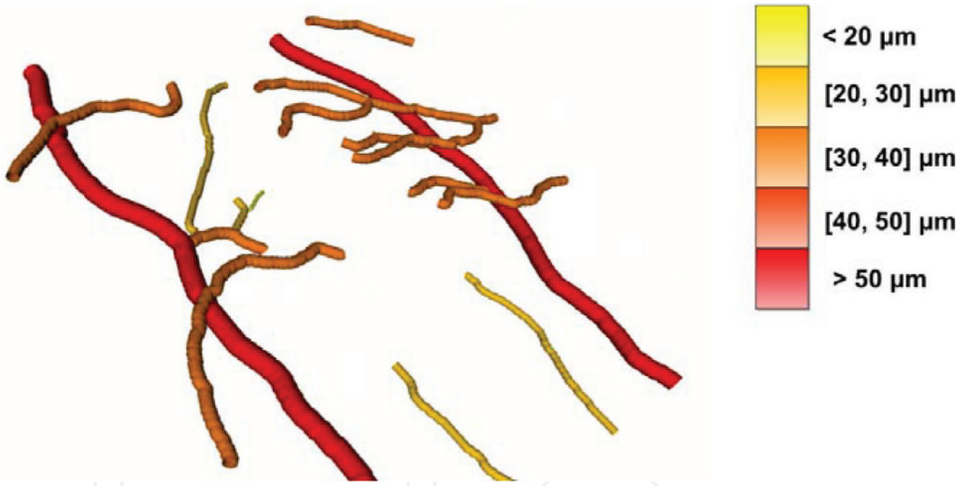

Figure 15. Representative example of the three-dimensional reconstruction of the retinal vessel tree in OCT images.

rotation, scaling and their arbitrary combinations. **Figure 15** shows a representative example of the three-dimensional reconstruction of the retinal vessel tree using the entire set of the OCT scans. The output image also presents the vessels by colors in terms of their calibers. The caliber scales are also presented to facilitate the analysis of the specialists.

3. Conclusions

The retina is a unique region of the human body where the blood vessels can be directly observed and analyzed in vivo and noninvasively. A precise identification and characterization of the retinal vasculature permit an early detection of the presence of several clinical characteristics that facilitate the diagnosis, prevention and treatment of many relevant

diseases that affect the retinal microcirculation, such as hypertension, diabetes or arteriosclerosis, among others.

CAD systems have become increasingly important in the assessment of outcomes in the daily clinical practice, mainly in the field of medical imaging-based diagnosis. These systems help the clinical experts in the analysis and interpretation of several modalities of medical images, facilitating and simplifying their work.

OCT is a noninvasive imaging modality capable of producing high-speed three-dimensional cross-sectional imaging of biological tissues with micron-level resolution. This medical image modality enables the precise evaluation of the retinal structure in real time, permitting the detection of alterations in the retinal microcirculation. The OCT devices provide two types of OCT images: the NIR retinography image and the OCT histological sections. These images are frequently acquired simultaneously by the same capture device.

In this chapter, we analyzed the characteristics of the OCT scans and their suitability for the vascular analysis. Additionally, we presented two different and independent approaches for the automatic identification and extraction of the retinal vascular structure to highlight the potential of these computational approaches in the field. The first approach uses the information provided by the NIR retinography image in combination with the histological sections. The second approach uses only the information provided by the OCT histological sections for the characterization of the vessel profiles. Then, both computational approaches perform the corresponding graphical two-dimensional or three-dimensional visual representation of the retinal vessel tree using the extracted information.

These fully automatic systems allow a more accurate and reliable visualization of the complex vascular structure of the retina, and consequently, make an improvement in the visual inspection and analyses of the retinal vessel tree. In addition, the vessel representation permits a more precise analysis of the retinal microcirculation, making the diagnosis of various retinal and systemic pathologies easier for doctors.

Acknowledgements

This work is supported by the Instituto de Salud Carlos III, Government of Spain and FEDER funds of the European Union through the PI14/02161 and the DTS15/00153 research projects and by the Ministerio de Economía y Competitividad, Government of Spain through the DPI2015-69948-R research project. Also, this work has received financial support from the European Union (European Regional Development Fund-ERDF) and the Xunta de Galicia, Centro singular de investigación de Galicia accreditation 2016-2019, Ref. ED431G/01; and Grupos de Referencia Competitiva, Ref. ED431C 2016-047.

Conflict of interest

The authors declare that they have no conflict of interest.

Author details

Joaquim de Moura[1,2], Jorge Novo[1,2]*, José Rouco[1,2], Noelia Barreira[1,2], Manuel Penedo[1,2] and Marcos Ortega[1,2]

*Address all correspondence to: jnovo@udc.es

1 Department of Computing, University of A Coruña, A Coruña, Spain

2 Research Center of Information and Communication Technologies (CITIC), University of A Coruña, A Coruña, Spain

References

[1] Wong TY, Mitchell P. Hypertensive retinopathy. New England Journal of Medicine. 2004;**351**(22):2310-2317. DOI: 10.1056/NEJMra032865

[2] Nguyen TT, Wong TY. Retinal vascular changes and diabetic retinopathy. Current Diabetes Reports. 2009;**9**(4):277-283. DOI: 10.1007/s11892-009-0043-4

[3] Klein R, Sharrett AR, Klein BE, Chambless LE, Cooper LS, Hubbard LD, Evans G. Are retinal arteriolar abnormalities related to atherosclerosis?: The Atherosclerosis Risk in Communities Study. Arteriosclerosis, Thrombosis, and Vascular Biology. 2000;**20**(6):1644-1650. DOI: 10.1161/01.ATV.20.6.1644

[4] Stevens GA, White RA, Flaxman SR, Price H, Jonas JB, Keeffe J, Leasher J, Naidoo K, Pesudovs K, Resnikoff S, Taylor H. Global prevalence of vision impairment and blindness: Magnitude and temporal trends, 1990-2010. Ophthalmology. 2013;**120**(12):2377-2384. DOI: 10.1016/j.ophtha.2013.05.025

[5] MacGillivray TJ, Trucco E, Cameron JR, Dhillon B, Houston JG, Van Beek EJ. Retinal imaging as a source of biomarkers for diagnosis, characterization and prognosis of chronic illness or long-term conditions. The British Journal of Radiology. 2014;**87**(1040):20130832. DOI: 10.1259/bjr.20130832

[6] Xu Z, Guo X, Hu X, Chen X, Wang Z. The identification and recognition based on point for blood vessel of ocular fundus. In: Proceedings of the International Conference on Biometrics: Advances in Biometrics (ICB 2006); 5-7 January 2006; Hong Kong, China. pp. 770-776

[7] Ortega M, Rouco J, Novo J, Penedo MG. Vascular landmark detection in retinal images. Lecture Notes in Computer Science (EUROCAST 2009); Feb 2009; Canary Islands, Spain. pp. 211-217. DOI: 10.1007/978-3-642-04772-5_28

[8] Ortega M, Penedo MG, Rouco J, Barreira N, Carreira MJ. Personal verification based on extraction and characterisation of retinal feature points. Journal of Visual Languages & Computing. 2009 Apr 1;**20**(2):80-90. DOI: 10.1016/j.jvlc.2009.01.006

[9] Mookiah MR, Acharya UR, Chua CK, Lim CM, Ng EY, Laude A. Computer-aided diagnosis of diabetic retinopathy: A review. Computers in Biology and Medicine. 2013 Dec 1;**43**(12):2136-2155. DOI: 10.1016/j.compbiomed.2013.10.007

[10] Novo J, Hermida A, Ortega M, Barreira N, Penedo MG, López JE, Calvo C. Hydra: A web-based system for cardiovascular analysis, diagnosis and treatment. Computer Methods and Programs in Biomedicine. 2017 Feb 1;**139**:61-81. DOI: 10.1016/j.cmpb.2016.10.019

[11] Adhi M, Duker JS. Optical coherence tomography—Current and future applications. Current Opinion in Ophthalmology. 2013 May;**24**(3):213. DOI: 10.1097/ICU.0b013e32835f8bf8

[12] Huang D, Swanson EA, Lin CP, Schuman JS, Stinson WG, Chang W, Hee MR, Flotte T, Gregory K, Puliafito CA. Optical coherence tomography. Science. 1991 Nov 22;**254**(5035):1178-1181. DOI: 10.1126/science.1957169

[13] Bourne RR, Flaxman SR, Braithwaite T, Cicinelli MV, Das A, Jonas JB, Keeffe J, Kempen JH, Leasher J, Limburg H, Naidoo K. Magnitude, temporal trends, and projections of the global prevalence of blindness and distance and near vision impairment: A systematic review and meta-analysis. The Lancet Global Health. 2017 Sep 1;**5**(9):e888-e897. DOI: 10.1016/S2214-109X(17)30293-0

[14] Michelson AA, Morley EW. On the relative motion of the earth and of the luminiferous ether. Sidereal Messenger. 1887;**6**:306-310. DOI: 10.1366/0003702874447824

[15] Kalev-Landoy M, Day AC, Cordeiro MF, Migdal C. Optical coherence tomography in anterior segment imaging. Acta Ophthalmologica. 2007 Jun 1;**85**(4):427-430. DOI: 10.1111/j.1600-0420.2007.00876.x

[16] Cabrera DeBuc D, Somfai GM, Koller A. Retinal microvascular network alterations: Potential biomarkers of cerebrovascular and neural diseases. American Journal of Physiology-Heart and Circulatory Physiology. 2016 Dec 6;**312**(2):H201-H212. DOI: 10.1152/ajpheart.00201.2016

[17] Fujimoto J, Swanson E. The development, commercialization, and impact of optical coherence tomography. Investigative Ophthalmology & Visual Science. 2016 Jul 1;**57**(9):1-3. DOI: 10.1167/iovs.16-19963

[18] Leite MT, Rao HL, Zangwill LM, Weinreb RN, Medeiros FA. Comparison of the diagnostic accuracies of the Spectralis, Cirrus, and RTVue optical coherence tomography devices in glaucoma. Ophthalmology. 2011 Jul 1;**118**(7):1334-1339. DOI: 10.1016/j.ophtha.2010.11.029

[19] de Moura J, Novo J, Charlón P, Barreira N, Ortega M. Enhanced visualization of the retinal vasculature using depth information in OCT. Medical & Biological Engineering & Computing. 2017;**55**(12):2209-2225. DOI: 10.1007/s11517-017-1660-8

[20] Jackway PT. Improved morphological top-hat. Electronics Letters. 2000;**36**(14):1194-1195. DOI: 10.1049/el:20000873

[21] Jin J, Yang L, Zhang X, Ding M. Vascular tree segmentation in medical images using Hessian-based multiscale filtering and level set method. Computational and Mathematical Methods in Medicine. 2013;**2013**. DOI: 10.1155/2013/502013

[22] Calvo D, Ortega M, Penedo MG, Rouco J. Automatic detection and characterisation of retinal vessel tree bifurcations and crossovers in eye fundus images. Computer Methods and Programs in Biomedicine. 2011 Jul;**103**(1, 1):28-38. DOI: 10.1016/j.cmpb.2010.06.002

[23] de Moura J, Novo J, Rouco J, Penedo MG, Ortega M. Automatic detection of blood vessels in retinal OCT images. In: Proceedings of the International Work-Conference on the Interplay Between Natural and Artificial Computation (IWINAC 2017); 19-23 Jun 2017; A Coruña. 2017. pp. 3-10. DOI: 10.1007/978-3-319-59773-7_1

[24] Masland RH. The fundamental plan of the retina. Nature Neuroscience. 2001;**4**(9):877. DOI: 10.1038/nn0901-877

[25] González-López A, Ortega M, Penedo MG, Charlón P. Automatic robust segmentation of retinal layers in oct images with refinement stages. In: Proceedings of the International Conference Image Analysis and Recognition (ICIAR 2014); 22-24 OCT 2014; Vilamoura, Portugal. 2014. pp. 337-345. DOI: 10.1007/978-3-319-11755-3_38

[26] de Moura J, Novo J, Ortega M, Charlón P. 3D retinal vessel tree segmentation and reconstruction with OCT images. In: Proceedings of the International Conference Image Analysis and Recognition (ICIAR 2016); 13 Jul 2016. pp. 716-726. DOI: 10.1007/978-3-319-41501-7_80

[27] de Moura J, Novo J, Ortega M, Barreira N, Penedo MG. Interactive three-dimensional visualization system of the vascular structure in OCT retinal images. In: Proceedings of the International Conference on Computer Aided Systems Theory (EUROCAST 2017); Feb 2017; Canary Islands, Spain. pp. 306-313. DOI: 10.1007/978-3-319-74727-9_36

IntechOpen